Chinese Chemical Letters 35 (2024) 108934

Contents lists available at ScienceDirect

Chinese Chemical Letters

journal homepage: www.elsevier.com/locate/cclet

Triphenylamine-AIEgens photoactive materials for cancer theranostics

Junjie Wang[c,d,1], Yan Wang[a,b,1], Zhengdong Li[e,1], Changqiang Xie[a,b], Musammir Khan[f], Xingzhou Peng[a,b,*], Fabiao Yu[c,d,*]

[a] State Key Laboratory of Digital Medical Engineering, School of Biomedical Engineering, Hainan University, Haikou 570228, China
[b] Key Laboratory of Biomedical Engineering of Hainan Province, One Health Institute, Hainan University, Haikou 570228, China
[c] Key Laboratory of Hainan Trauma and Disaster Rescue, The First Affiliated Hospital of Hainan Medical University, Hainan Medical University, Haikou 571199, China
[d] Engineering Research Center for Hainan Bio-Smart Materials and Bio-Medical Devices, Key Laboratory of Emergency and Trauma, Ministry of Education, Key Laboratory of Hainan Functional Materials and Molecular Imaging, College of Emergency and Trauma, Hainan Medical University, Haikou 571199, China
[e] Precision Medical Center, Guangyuan City Centre hospital, Guangyuan 628099, China
[f] School of Natural Sciences (SNS), National University of Science and Technology (NUST), H-12, Islamabad 44000, Pakistan

ARTICLE INFO

Article history:
Received 15 June 2023
Revised 10 August 2023
Accepted 14 August 2023
Available online 15 August 2023

Keywords:
Triphenylamine
AIEgens
Targeting
Theranostics
Phototherapy
Immunotherapy

ABSTRACT

Triphenylamine (TPA)-based aggregation-induced emission luminogens (TPA-AIEgens), a type of photoactive material utilizing the typical TPA moiety, has recently attracted increasing attention for the diagnostics and treatment of tumors due to their remarkable chemo-physical performance in optoelectronic research. TPA-AIEgens are distinguished from other photoactive agents by their strong fluorescence, good sensitivity, high signal-to-noise ratio, resistance to photobleaching, and lack of high concentration or aggregation-caused fluoresce quenching effects. In this review, we summarize the current advancements and the biomedical progress of TPA-AIEgens in tumor theranostics. First, the design principles of TPA-AIEgens photoactive agents as well as the advanced targeting strategies for nuclei, cell membranes, cell organelle and tumors were introduced, respectively. Next, the applications of TPA-AIEgens in tumor diagnosis and therapeutic techniques were reviewed. Last, the challenges and prospects of TPA-AIEgens for cancer therapy were performed. The given landscape of the TPA-AIEgens hereby is meaningful for the further design and utilization of the novel photoactive material, which could be beneficial for the development of clinic applications.

1. Introduction

Malignant tumors are the primary cause of human mortality, which represent a severe threat to human health and survival [1]. Nowadays, surgery, radiation, and chemotherapy are the three primary traditional treatments. Unfortunately, these traditional treatments suffer defects, such as significant systemic side effects and high recurrence rates [2,3]. Recently, phototheranostics have made significant contributions to cancer treatment due to their light-controllability, non-invasiveness, specific target, low toxicity and good selectivity [4–6]. Normally, photodynamic therapy (PDT) and photothermal therapy (PTT) are two types of phototherapies that exogenous photosensitizing agents are involved to selectively kill tumors or inhibit tumor growth with light radiation [7,8]. In PDT, photosensitizers (PSs) are typically used to generate cytotoxic reactive oxygen species (ROS), such as singlet oxygen ($^1O_2$), superoxide ($O_2\bullet^-$) and hydroxyl radical (•OH), which is able to eliminate tumor cells [5,9]. Photothermal agents can enhance the heating process of cells and tissues in the local area by absorbing laser energy and converting it into heat [10–12], which is similar to laser therapy [13]. The main discrepancy is that laser therapy uses endogenous chromophores with non-selectivity towards malignant cells, while PTT with exogenous agents can specifically target cancer cells. With the aid of photoactive agents, both the PDT and PTT can produce vigorous interaction with biological substances, leading to the immunogenic cell death (ICD), vascular injury, and immunological response [14–17].

Recently, the photoactive agents based on AIE luminogens (AIEgens) developed by Tang Benzhong's research group have made breakthroughs in phototherapy research. An interesting phenomenon termed aggregation-induced emission (AIE) occurs when a series of non-emissive molecules in the dispersed state are induced to show strong emission upon aggregate formation or in solid state [18]. Due to the existence of the strong electron-vibration coupling in the dispersed state, AIE molecules

* Corresponding authors.
E-mail addresses: pengxzh@hainanu.edu.cn (X. Peng), yufabiao@hainmc.edu.cn (F. Yu).
[1] These authors contributed equally to this work.

https://doi.org/10.1016/j.cclet.2023.108934
1001-8417/

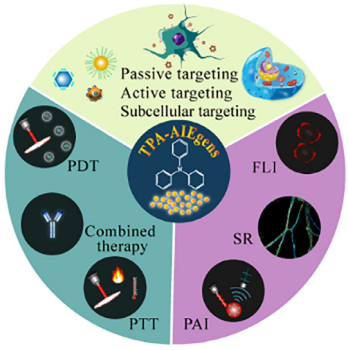

Scheme 1. TPA-AIEgens for cancer theranostic, including targeting strategies, biological imaging and cancer treatment.

demonstrate the intrinsic non-radiative transitions and fluorescence quench. In the aggregated state, the molecular environment's restriction of intramolecular movements (RIM) might impair the electron-vibrational coupling of molecular system, resulting in depressed non-radiative transitions and enhanced fluorescence [19,20]. In general, the clinical diagnostic agents (*e.g.*, indocyanine green, porphyrin) suffer from certain problems such as aggregation-induced fluorescence quenching (ACQ) and photobleaching [21,22]; while AIEgens offers the following benefits compared to the traditional fluorescent dyes: (1) High-intensity fluorescence; (2) efficient light conversion; (3) strong stability; (4) luminescence regulation by flexible chemical modification; (5) high resolution in biological imaging [23,24].

The fundamental AIE motifs, such as tetraphenylene (TPE), triphenylamine (TPA), 2,3,4,5-tetraphenylsiloles (TPS), phenylvinyl anthrance and phenyl substituted pyrrole, are integral to the creation of AIE materials [25]. In contrast to typical TPE-AIEgens, TPA-AIEgens is more flexible to be designed for *in vivo* applications such as high water-solubility and strong near-infrared II (NIR-II) absorption. The chemical structure of TPA is composed of three benzene rings and a central nitrogen atom. Due to its unique helical structure and three phenyl rotors, TPA not only plays a role as the strong electron donor but also acts as a molecular rotor, making it easy to construct a variety of TPA-AIEgens. As an electron donor, TPA is combined with an electron acceptor to obtain a molecule with donor-acceptor (D-A) structure resulting in an adjusted intramolecular push-pull electron interaction, which benefits the red-shift of fluorescence and/or enhances intersystem crossing (ISC) process to generate more ROS [25,26]. When acting as a molecular rotor, the highly distorted conformation of TPA increases the molecular distance, reducing the intermolecular π-π packing and retaining the intramolecular rotation, which is beneficial to promote fluorescence and/or heat generation [27,28]. Therefore, TPA is a crucial functional segment in the construction of TAP-AIEgens.

Up to now, TPA-AIEgens have been developed as novel molecular materials with photosensitive and photothermal capabilities, demonstrating the huge potential in tumor theranostics [29]. Thus, the design principles, targeting strategies, and the latest progress in biological imaging and treatment based on TPA-AIEgens photoactive agents are summarized in this minireview (Scheme 1). First, the principles of design TPA-AIEgens with near-infrared absorption and good biocompatibility were summarized. Next, TPA-AIEgens targeting strategies, including targeting to nuclei, cell membranes, cell organelles and tumors, were presented. Then it introduced the application of TPA-AIEgens in biological imaging and phototherapy for the most recent years. Finally, the photoactive agents based on TPA-AIEgens for cancer treatment were prospected. We hope this review can provide valuable information for design and application of TPA-AIEgens to accelerate their clinical translation.

2. The design principles for TPA-AIEgens photoactive agents

The three benzene rings and a central nitrogen atom make up the structure of TPA. TPA does not naturally emit fluorescence, but it can be used to create AIE compounds due to its helical structure and strong electron donating capacity [30,31]. According to Jablonski diagram, organic molecules migrate from the ground state (S_0) to the single excited state (S_1) upon light absorption. The excited state then returns to S_0 state by releasing energy *via* radiative decay to produce fluorescence, or *via* internal conversion (IC) to yield heat. The ISC between S_1 and triplet excited state (T_1) happens when their energy gap is tiny or when their spin orbit coupling effect is strong. Nevertheless, T_1 can react with the surroundings to yield ROS such as singlet oxygen ($^1O_2$), free radicals ($O_2^{\bullet-}$, •OH) owing to its much longer lifetime than S_1 [32–35]. Thus, the photophysical properties of TPA-AIEgens can be tailored *via* elegant molecular design. Besides, the TPA-AIEgens can not only be used as excellent luminescent materials, but also render more exciting functions like photosensitizer, photothermal/photoacoustic agents [36–39].

TPA is the core unit with good electron-donating performance, providing a flexible platform for constructing AIEgens. The basic design strategies of TPA-AIEgens are to build a twisted π system by introducing electron acceptor (A) and electron donor (D) to RIM [40]: (1) Conjugation of different electron withdrawing units to tune the absorption/emission wavelength; (2) Build of various molecular backbone to meet the desired functions; (3) Enhancement of the steric hindrance of molecules to adjust molecular non-radiative attenuation properties.

The structure of typical TPA-AIEgens were presented in Fig. 1. The prolongation of π-conjugation system and/or strengthening of acceptor ability are main approach to endow TPA-AIEgens with long-wavelength absorption/emission. The thiophene unit, as demonstrated in the compounds **2** and **3**, is commonly used as π bridge [27]. To obtain high fluorescence quantum yield and drive the emission wavelength to the NIR-II region, benzo[1,2,5]thiadiazole (BT) and benzobisthiadiazole (BBT) are typically utilized as strong acceptors (like compounds **4** and **8**) [41,42]. Moreover, the steric hindrance is also an efficient approach to obtaining bright NIR fluorescence. The introduction of the steric hindrance by rigid backbone has been successfully used to obtain high fluorescence emission quantum yield. Compared with compound **4**, the rigidity of compound **5** was increased due to hydrogen bond formation between additional benzene ring and BT core. A highly twisted D-A conformation in the excited state is stimulated, favoring the creation of the intramolecular charge transfer (ICT) state to yield a high fluorescence quantum yield (compound **4**: ϕ_{fl} = 0.45; compound **5**: ϕ_{fl} = 0.6) [43]. The introduction of steric hindrance caused by *ortho*-substituted alkylthiophene encouraged the development of dark twisted intramolecular charge transfer (TICT) state to achieve a considerably red-shifted emission wavelength, as utilized in compounds **6**–**8** [44]. Besides the radiative decay, nonradiative decay could be used for other functional materials such as PS, photothermal agents. Reducing the energy gap between the S_1 and T_1 (ΔE_{st}) and enhancing ICT effect could yield promoted ISC, which are more suitable to create radicals or singlet oxygen for PDT. For example, compound **9** (tTID) and compound **10** (tTDCR) have been synthesized to show ΔE_{st} values of 0.06 and 0.3 eV, respectively. Accompanied by declining in the ΔE_{st} values, tTDCR showed a greater capacity to produce ROS upon light irradiation in comparison with tTID [45]. Manipulating the TICT state *via* activating molecular motion in aggregates was verified as a powerful strategy to meet the demand of photoacoustic imaging (PAI) as

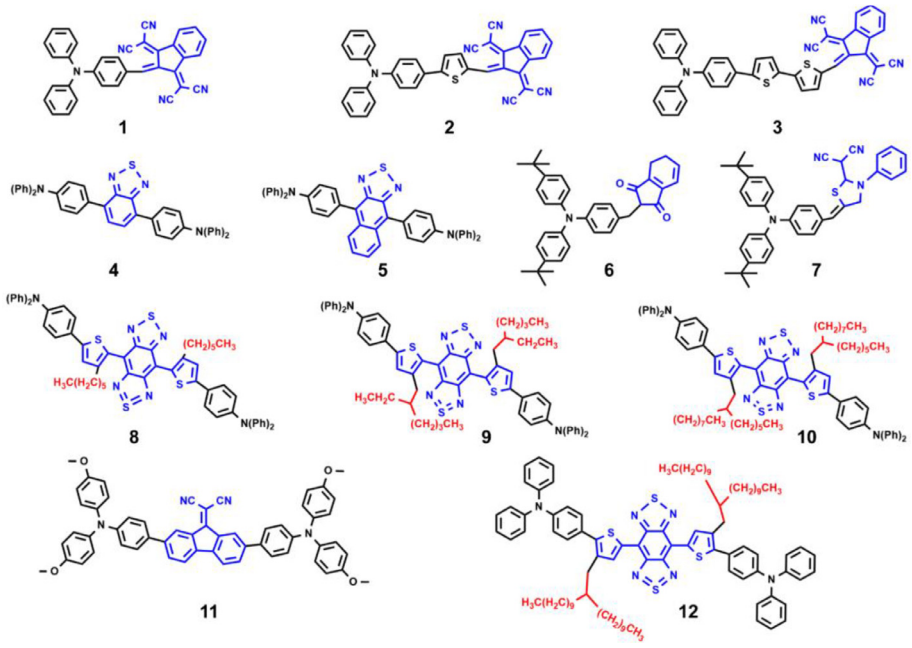

Fig. 1. Typical TPA-AIEgens used for cancer diagnosis and treatment. Compounds **1**–**3** with extended π system to obtain the red-shifted and high fluorescence emission; compounds **4** and **5** with rigid and strong acceptor unit to promote the fluorescence quantum yield; compounds **6** and **7** with low ΔE_{st} values to enhance ROS generation; compounds **8**–**10** with increased steric hindrance to red shift to NIR II emission; compounds **11** and **12** with TICT state to boost photothermal conversion property.

well as PTT. The strong D-A structure (like compound **11**) and additional long-branched alkyl chains (like compound **12**) make the molecular motion easy and lose intermolecular packing, resulting in a boost of photothermal conversion property [46,47].

3. The targeting strategies for TPA-AIEgens photoactive agents

With the in-depth understanding of tumor biology and mechanism based on tumor diagnosis and treatment, the precise delivery of photoactive agents to the tumor sites or specific organelles is a prerequisite for efficient cancer treatment [48–50]. Given the favorable characteristics of TPA-AIEgens, many researchers have developed a variety of photoactive agents targeting tumor foci, nuclei and organelles in accordance with the types of TPA-AIEgens. These TPA-AIEgens have been widely applied for biological imaging and phototherapy, which can minimize the damage to health tissues and reduce non-specific drug toxicity and achieve the accurate treatment.

3.1. Strategies for intracellular localization

Organelle targeted probes have greatly increased therapeutic efficacy, which has garnered growing interest recently [51–53]. Herein, we focus on the organelle-targeted probes based on TPA-AIEgens framework. The structure-inherent targeting (SIT) strategy refers to the specific natural targeting ability of the molecule itself [54]. The overall electric charge (Z) and suitable logarithm of the octanol-water partition coefficient (log*P*) could provide principle for design photoactive agents with specific targeting towards tissue, cells and organelles [37,55,56]: (1) The molecule probes with a log*P* value between 0 and 8 and anioic properties are able to be accumulated in nuclei; (2) A log*P* value between 0 and 5 and cationic properties allow the molecular to accumulate more in mitochondria; (3) The higher log*P* endows cationic molecules with the localization at endoplasmic reticulum (ER); (4) With a negative log*P* value and cationic properties, the molecule can be taken up by lysosomes. Furthermore, recognition groups, targeting groups and fluorophores make up the majority of the components of organelle-targeting probes.

Generally, to achieve accumulation at nuclei, the probe can be designed either by binding to the DNA, or by binding to the histone basic proteins. Platinum(II) complexes is commonly utilized as the DNA binding agents, conjunction of trinuclear platinum to the TPA moiety can yield a nuclear target AIE probe. This probe triggered DNA damage reactions, arrested the cell cycle in the G2/M phase, and ultimately caused cell death [57]. In addition, intranuclear enzyme and nucleic acids are the potential target sites. The cationic pyridine units and hydroxamic acid chelating group endow the AIE probe (MeTPAE) molecule with the capacities of nucleic acid binding and the zinc ions chelating respectively, which could cause obvious cell cycle arrest and show outstanding PDT anti-tumor effectiveness (Fig. 2a) [58].

Cell membrane is another favorite targeting site. To enrich at the cell membrane, the probe should endow superamphiphilic structure properties, which can be bound to membrane proteins [63]. The pyridine cationic unit is typically used for precisely cell membrane targeting. With this functional group, the probe TBMPEI was able to selectively accumulate on the cell membrane and significantly induce cell necroptosis upon irradiation by light (Fig. 2b) [59].

The overproduction of ROS in mitochondria may result in oxidative stress, which may disturb the microenvironment of mitochondrial and result in apoptosis, autophagy and necroptosis [64]. Thus, the mitochondrion is an important organelle for PDT. There are two basic approaches for targeting mitochondria. Building a positive charge structure is one option, while using mitochondria-specific peptides is another. Generally, the triphenylphosphonium (TPP) cation, trimethylphenylammonium hexafluorophosphate [65] and quaternary ammonium units [66] server as mitochondria-targeting lipophilic cationic ligands, which display the potential of electrostatic attraction with the mitochondrial membrane. While the TPA-AIEgens probe with a higher hydrophobicity and a cation strategy is preferring to accumulate in ER membranes after extended incubation [6,67]. In addition, ROS-induced stress in the ER may activate downstream immunological pathways, causing cells through

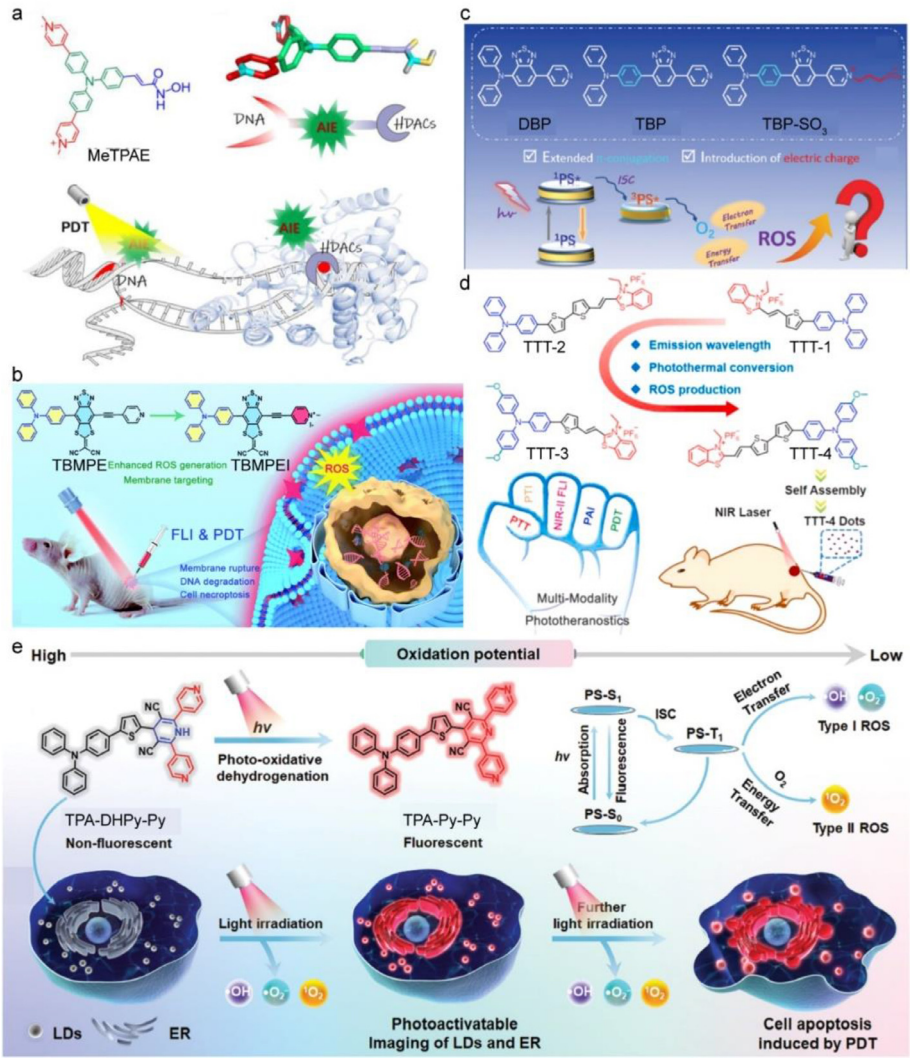

Fig. 2. (a) Schematic illustration of MeTPAE with nuclei-targeting function for PDT. Reproduced with permission [58]. Copyright 2022, Wiley-VCH. (b) Schematic illustration of molecular design diagram of a high-performance AIE photosensitizer with cell membrane-targeting function for fluorescence imaging-guided PDT. Reproduced with permission [59]. Copyright 2022, The Royal Society of Chemistry. (c) Schematic illustration of the structures of DBP, TBP and TBP-SO_3. Reproduced with permission [60]. Copyright 2022, The Royal Society of Chemistry. (d) Schematic illustration of the structures of TTT-1, TTT-2, TTT-3 and TTT-4. Reproduced with permission [61]. Copyright 2021, Elsevier. (e) Schematic diagram of the structure of 1,4-dihydropyridine derivatives for both LD and ER-targeting imaging and therapy. Reproduced with permission [62]. Copyright 2023, Wiley-VCH.

immunogenic death [68]. Typically, modification of specific peptides or methyl sulfonamide can endow probe with ER-targeting abilities. A TPA-AIEgens (TBP-SO_3) showed a comparable Pearson coefficient in compare to ER-Tracker Red ($P = 0.93$) (Fig. 2c) [60].

The probe accumulated in lysosomes can be driven by pinocytosis, ion trapping of weak bases, precipitation trapping of weak acids, or binding to lipid or protein [69]. The morpholine and other amine groups are the two classical moieties that serve as functional groups for the most lysosomes targeting [27,70]. A probe named TTT-4, displayed a powerful lysosomal targeting ability, meanwhile performed better photoacoustic guided imaging ability (Fig. 2d) [61].

3.2. Strategies for the multi-organelle targeting

To obtain better therapeutic effect, the drugs with the capability of multi-organelle-targeting are more attractive than those targeting to specific organelle. Therefore, increased attention has been donated to the structural design of TPA-AIEgens for the improvement of clinical outcome. A TPA-AIEgens (DTPAP-P) with TPA and pyridine (P) was reported by Tang's group. This cationic DTPAP-P can specifically target to mitochondria in the live cell, and to nuclei when the cells were fixed, which provide a promising probe in stimulated emission depletion (STED) nanoscopy for the tunable organelle-specific imaging and dynamic monitoring in nanometer scale [71].

Recently, the substituent effect was used to create a series of TPA derivatives based on 1,4-DHPy as the photo-responsive group. With additional pyridine, the TPA-DHPy-Py can target to lipid droplets and ER accompanying with the high ROS generation under the laser irradiation, which result in high photoactivation efficiency and excellent photodynamic activity. TPA-DHPy-Py can provide precise and tunable tumor phototherapy medications by enabling *in situ* real-time monitoring of the lipid droplet fusion process and endoplasmic reticulum vacuolation under oxidative stress during the light irradiation process (Fig. 2e) [62].

3.3. Strategies for tumor targeting

Tumor targeting of TPA-AIEgens is typically realized by their nanocarriers. Various factors, such as the size, shape, surface charge, hydrophobicity, rigidity, and surface-conjugated ligand,

determine the fate of TPA-AIEgens in the tumor cells. With the aid of nanocarriers, the targeting strategies are normally classified into two kinds, one is passive targeting, the other is active targeting [72].

By altering the size, shape, charge in accordance with the enhanced permeability and retention (EPR) effect, the passive targeting to tumor site can be accomplished. The uniform spherical structure of nanoparticles (NPs) with an average diameter of 50–200 nm can be effectively accumulated at tumor sites [73]. The probe (TPA-T-TQ ONPs) encapsulated in the 1,2-distearoyl-*sn*-glycero-3-phosphoethanolamine-*N*-[methoxy(polyethylene glycol)-2000] (DSPE-PEG_{2000}) with an average diameter of 56 nm were enriched in tumor *via* EPR delivery strategy [74]. Due to the negative charge of tumor cells, the probe with positive charges will benefit to accumulation of NPs in tumor site. Incorporation of pH response polymer (*e.g.*, poly(β-amino ester)-*b*-poly(caprolactone)) on the surface of NPs, the NPs could be efficiently delivery to tumor site *via* electronstatic binding force [46].

However, TPA-AIEgens with the passive target strategy can kill tumor cells and normal indiscriminately, leading to strong side effect such as systemic toxicity. Active targeting strategies is increasingly preferred to improve targeting specificity. Generally, the surface of NPs can be modified with biological ligands targeting tumor cell-specific receptors to achieve precise delivery of the cargoes. For example, CD44 is overexpressed on tumor cells surface, hyaluronic acid (HA) can bind to CD44 through specific affinity. Thus, HA can be employed as an active targeting moiety, linked to hydrophobic oligomer or self-assembled to lipid layer [75].

4. Biological imaging based on TPA-AIEgens

Tumor visualization can accurately locate the tumor site and define its spread degree, which is helpful for better clinical diagnosis and treatment of tumors [76,77]. Designing therapeutic agents with inherent image tracking property is therefore extremely desired to monitor and visualize the therapeutic effects. This section only discusses some representative works of TPA-AIEgens as contrast agents for fluorescence imaging and fluorescence/photoacoustic dual-modality imaging in recent five years.

4.1. Fluorescence imaging (FLI)

AIEgens has emitted bright fluorescence to satisfy the particular and stringent requirements of various applications, such as noninvasiveness, high sensitivity, easy operation, real-time tracking [78–80]. In situ monitoring fundamental physical process make it possible to optimize treatment individually. In 2021, Zhu *et al.* reported a TPA-AIEgen (TPA-DPPy) for real-time fluorescence detection of tumor cells, which has a novel structure of D-A pyridinium salt [81]. To improve uptake by tumor cells, TPA-DPPy was incorporated into the low density lipoprotein (LDL) particles and efficiently delivered into mitochondrial *via* LDL receptor-mediated endocytosis. As the illumination time increased, the fluorescence intensity was significantly enhanced, and the morphology of the cells underwent significant changes, including chromatin condensation, cells shrinking from expanded 3 dimensional (3D) structures to flat 2 dimensional (2D) shapes, which provide a real-time fluorescence feedback for tumor treatment. To improve the penetration and imaging depth of light to biological tissues, two-photon fluorescence imaging (2P-FLI) based on TPA-AIEgens was developed [82,83]. TBP-Au, a powerful AIEgens, was prepared by integrating an anticancer Au (I) moiety with an AIE-active photosensitizer (TBP), which exhibited a large two-photon absorption cross section at 870 nm and reached a deeper imaging depth compared to single-photon imaging (imaging depth up to 170 μm) (Figs. 3a–c). Therefore, TBP-Au with two-photon imaging showed a better resolution and greater signal-to-noise ratio for tumor fluorescence tracking [84]. Liu also investigated a two-photon photoactive agent TPA-2PI for dual-targeted DNA and mitochondria imaging. It was demonstrated to penetrate deeper cells (24 μm) and abdominal blood vessels (384 μm) layers and to create a green fluorescence signal when activated at 960 nm [85].

4.2. Fluorescence and photoacoustic dual-modality imaging (FLI/PAI)

PAI is a new biomedical imaging modality, which converted the absorbed laser energy into ultrasonic waves by intrinsic or extrinsic contrast agents in the tissue, thus providing *in vivo* imaging information in high penetration depths [87,88]. However, the low sensitivity and poor spatial resolution are the defects of PAI. TPA-AIEgens combined with FLI/PAI dual modalities in one probe would be unambiguously conducive to obtain wealthy and precise tumor information, which is highly demand in modern life science research [86,89]. In 2021, Tang's group have demonstrated a hypoxia response probe TBTO that consisted of a TPA-BTD-TPA derivative with four diethylamino *N*-oxide groups [86]. The TBTO had a typical donor-acceptor-donor (D-A-D) structure and a strong TICT effect, which allowed red shift of fluorescence emission to the NIR region and generated a strong PA signal. The *in vivo* dual-mode imaging of specific tumor microenvironments was verified these properties (Figs. 3d and e). Recently, Peng *et al.* designed and synthesized a photoactive agent CyQN-BTT with a donor-π-acceptor (D-π-A) structure [90]. Both electron-deficient 2,1,3-benzothiadiazole and a π-bridge in CyQN-BTT were contributed to enhance charge transfer, promote non-radiative transition and red shift the emission to NIR-II region (938 nm). With the guidance of NIR-II FLI and PAI, CyQN-BTT were precisely delivery to tumor site and serves as a phototheranostic agent to treat cancer.

5. Cancer treatment based on TPA-AIEgens

By incorporating functional groups, the TPA-AIEgens can be designed into various photoactive agents used for cancer treatment, which benefit from red-shifted NIR absorption and emission, increased ROS generation, and higher photothermal conversion efficiency [27,91]. Many research have demonstrated the effectiveness of TPA-AIEgens as phototherapeutic agents for PDT, PTT and combination therapy to achieve the best therapeutic effect on tumors and avoid tumor metastasis and recurrence [92–94]. In this section, the most recent progress of TPA-AIEgens-based photoactive agents in PDT, PTT and combination therapies for tumor treatment were discussed.

5.1. Photodynamic therapy

In PDT, PS are used to produce ROS and kill tumor cells under light irradiation [95]. To improve the efficiency of PDT, subcellular targeting has become a promising strategy to deliver drugs. A series of TPA-AIEgens (TPA-TPP, Br-TPA-TPP, MeO-TPA-TPP and OPY-TPA-TPP) with dual-cationic fluorophores were designed by Tang's group, showing superior killing efficiency on cancer cells due to their mitochondria-target abilities [96]. *In vivo* experiment further verified that MeO-TPA-TPP can substantially inhibit tumor growth (Figs. S1a–e in Supporting information). The monitor and regulation of oxidative stress in lipid droplets (LD) and ER are of vital importance. The photoactivatable fluorescent probe TPA-DHPy with a 1,4-dihydropyridine moiety can quickly transform into its pyridine counterpart TPA-Py through photo-oxidative dehydrogenation. Under the white light irradiation, the probe demonstrated a high ROS generation efficiency. Furthermore, the in situ generated TPA-Py can drastically kill tumor cells by disrupting the function of LD and ER [62]. By rationally modifying the 1,4-DHPy substituent groups,

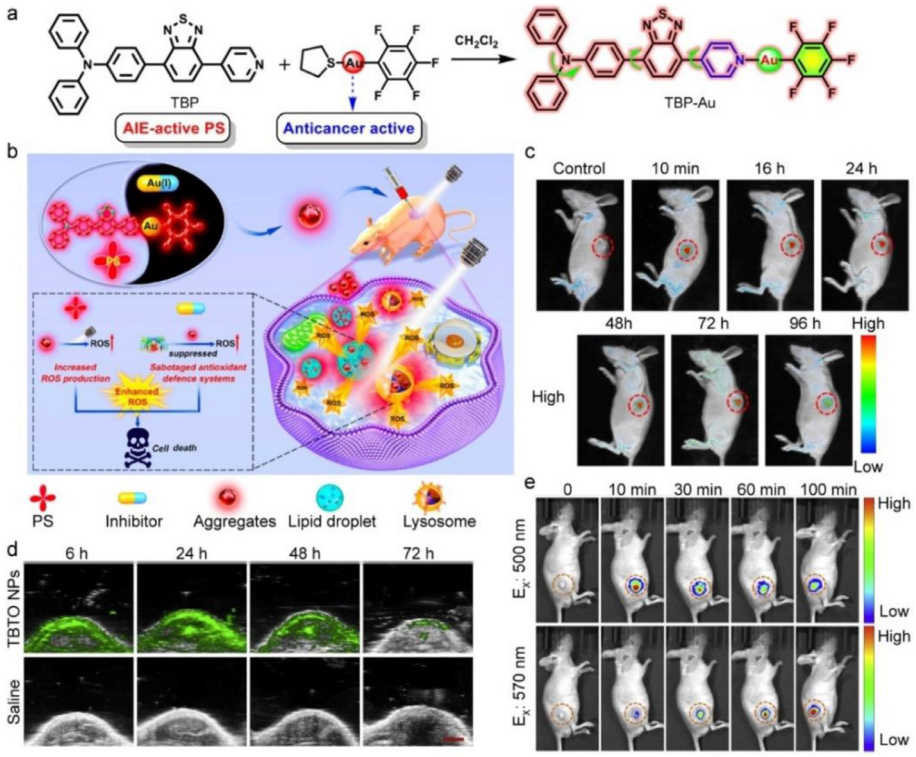

Fig. 3. (a) Molecular design and synthetic route of TBP-Au. (b) Schematic illustration of TBP-Au for anticancer therapeutics through synergistic effects of photodynamic therapy and thioredoxin reductase (TrxR) inhibition. (c) *In vivo* real-time fluorescence imaging in HeLa tumor-bearing nude mice after intratumor injection of TBP-Au (λex: 530 nm). Reproduced with permission [84]. Copyright 2021, American Chemical Society. (d) *In vivo* real-time PA images of the tumor site in the mice after tail intravenous injection with TBTO NPs. (e) *In vivo* real-time NIR fluorescence imaging in tumor site after intratumoral injection with TBTO NPs. Reproduced with permission [86]. Copyright 2021, Elsevier.

a new finely engineered TPA-DHPy-Py AIEgen was synthesized and exhibited a lower oxidation potential, higher photoactivation efficiency, and smaller singlet-triplet energy gaps than TPA-DHPy [97], which demonstrated excellent PDT performance (Figs. S1f and g in Supporting information).

5.2. Photothermal synergistic therapy

In PTT, exogenous photothermal agents with high photothermal conversion efficiency can generate localized heat, thus providing the opportunity for tumor ablation [98–101]. As an ideal photothermal agents, TPA-AIEgens should demonstrate negligible fluorescence and enhanced nonradiative transition energy, which can be realized by increased ICT effect. For example, the TPA moiety was conjugated to electron-deficiency thiadiazoquinoxaline moiety to yield TPA-T-TQ [74]. The enhanced ICT effect bestows the TPA-T-TQ with a NIR absorption from 700 nm to 900 nm and excellent photothermal conversion performance. Then, nanoprecipitation technique was employed to form TPA-T-TQ NPs in order to introduce TPA-T-TQ into aqueous media. The excellent photothermal ability of TPA-T-TQ NPs has also been proved effective in killing tumor cells *via* a rapid temperature increase in the tumor site *in vivo* [70]. Since the effectiveness of PDT or PTT alone is constrained, the synergistic use of PDT and PTT is considered as a promising strategy to overcome their shortcomings to maximize the therapeutic effects of tumor treatment [102,103]. Tang *et al.* chose 9,10-phenanthrenequinone (PQ) conjugated with TPA derivatives to create a series of PSs with D-A-D structure [104]. Because of strong electron-withdrawing ability and intramolecular bond stretching vibration of PQ, these PQ-cored photosensitizers showed the outstanding photothermal conversion efficiency (37.1%) and highly effective ROS generation. In addition, these PQ derivatives fabricated nanoagents showed great potential for Type I photodynamic and photothermal combined antitumor therapy, as verified by both *in vitro* and *in vivo* experiments (Figs. S2a–d in Supporting information). The diketopyrrolopyrrole (DPP) can also be used for construction multifunctional photoactivator. The created TPA-TDPP NPs enabled NIR fluorescence image-guided PDT and PTT synergistic treatment due to its near-infrared fluorescence, excellent photodynamic therapy efficiency ($^1O_2$ quantum yield: 50%) and strong photothermal conversion ability (38.7%) (Figs. S2e–h in Supporting information) [105].

5.3. Phototherapy combined with immunotherapy

Only PDT or PTT treatment can hardly trigger systemic immune response and eliminate the tumor completely, thus phototherapy combined with immunotherapy can boost ICD effect induced by phototherapy and achieve better treatment effect [106,107]. To overcome the immunosuppression of tumor microenvironment and boost immune response, reprogramming tumor-associated macrophages is a promising strategy. Li's group designed a TPA-AIEgens PS with a D-A structure named tTDCR with a high ROS-generating efficiency. This probe was able to reprogram the macrophages from a pro-tumor type (M2) to an anti-tumor state (M1) *via* stimulating the nuclear factor κB (NF-κB) signaling pathway. *In vivo* experiments have proved that tTDCR can activate photodynamic immunotherapy for efficient tumor growth inhibition [45]. In addition, the type I PS could induce the ICD of tumor cells, reverse the immunosuppressive microenvironment, and promote the infiltration of $CD4^+$ and $CD8^+$ T cells even in hypoxic tumors environment [108].

The immune checkpoint blockers are also used for synergistic tumor therapy. Tang *et al.* designed a novel PS called α-Th-TPA-PIO

Table 1
The summary of TPA-AIEgens for tumor theranostics.

Name	Absorption/emission	Target	Diagnosis	Therapeutics	Tumor model	Ref.
β-TPA-PIO	405 nm/543 nm	Endoplasmic reticulum	FLI	PDT	SKOV3 subcutaneous tumor model	[6]
tTDCR	488 nm/627 nm	Tumor	FLI	PDT + immuno-therapy	4T1 subcutaneous tumor model	[45]
Tri(3-pyridylphenyl)amine	405 nm/480–580 nm	Nucleus	FLI	PDT	HeLa xenograft tumor model	[57]
MeTPAE	405 nm/600 ± 20 nm	Nucleus	FLI	PDT	4T1 subcutaneous tumor model	[58]
TBMPEI	465 nm/780 nm	Cell membrane	FLI	PDT	4T1 subcutaneous tumor model	[59]
$TPANPF_6$	405 nm/520–650 nm	Mitochondrion	FLI	PDT	/	[65]
TPATrzPy-3+	405 nm/570–650 nm	Mitochondrion	FLI	PDT	Zebrafish model of liver tumor	[66]
T-BDP	363, 631 nm/724 nm	Lysosome	FLI	PDT + PTT	/	[70]
DTPAP-P	456 nm/543 nm	Nucleus	FLI	PDT	/	[71]
TPA-DHPy-Py	488 nm/600–700 nm	Endoplasmic reticulum and lipid droplets	FLI	PDT	MDA-MB-231 subcutaneous model	[62]
BDPTPA	808 nm/-	Tumor	PAI	PDT + PTT	143B xenograft tumor model	[73]
TPA-T-TQ	780 nm/-	Tumor	PAI	PTT	4T1 subcutaneous tumor model	[74]
Ce6@HA-Cys-TTDTT	635 nm/700–750 nm	Tumor	NIR FLI	PDT + PTT	HeLa subcutaneous tumor model	[75]
TPA-DPPy	405 nm/-	Saturated fatty acids and mitochondrion	FLI	PDT	/	[81]
TBP-Au	488, 870 nm/575–630 nm	Lysosome and lipid droplets	2P-FLI	PDT	HeLa subcutaneous tumor model	[84]
TPA-2PI	960 nm/600–800 nm	DNA and mitochondrion	2P-FLI	PDT	4T1 subcutaneous tumor model	[85]
CyQN-BTT	671, 800 nm/900–1100 nm	Tumor	NIR-II FLI+PAI	PDT + PTT	4T1 subcutaneous tumor model	[90]
MeO-TPA-TPP	455 nm/550–620 nm	Mitochondrion	FLI	PDT	4T1 breast tumor model	[96]
TPA-DHPy	488 nm/500–650 nm	Endoplasmic reticulum and lipid droplets	FLI	PDT	HeLa subcutaneous tumor model	[97]
PQ-TPAOC1 NPs	660 nm/-	Tumor	/	PDT + PTT	4T1 tumor model	[104]
TPA-TDPP	638 nm/743 nm	Tumor	FLI	PDT + PTT	HeLa tumor model	[105]
TPA-DCR	460 nm/620 ± 25 nm	/	FLI	PDT + immuno-therapy	4T1 subcutaneous tumor model	[108]
α-Th-TPA-PIO	465 nm/660 nm	Endoplasmic reticulum	FLI	PDT + immuno-therapy	B16-F10 subcutaneous tumor model	[109]
Platinum(II) TPA	405 nm/620 ± 20 nm	Mitochondrion	FLI	PDT + immuno-therapy	U14 subcutaneous tumor model	[110]
DCP-PTPA	680 nm/-	Tumor	PAI	/	4T1 xenograft tumor model	[111]
BOPHY-2TPA	561 nm/630–690 nm	HeLa cell	FLI	PDT	/	[112]

that can selectively accumulate in ER and cause ER stress, further leading to effective ICD. When combined with anti-programmed death-ligand 1 (anti-PD-L1), PDT and immune checkpoint blockade work together synergistically to produce a robust systemic immunological response (Figs. S3a–d in Supporting information) [109]. Another powerful immunotherapeutic strategy for the treatment of tumor is the activation of the cyclic GMP-AMP synthase-stimulator of the interferon gene (cGAS-STING) pathway. Two Pt(II) complexes (Pt1 and Pt2) incorporating alkylated TPA ligand L were designed, which was the first photoactivator of the cGAS-STING pathway. Upon light irradiation, Pt1 and Pt2 damaged mitochondrial/nuclear DNA and nuclear membrane, and induced pyroptosis in tumor cells, which in turn stimulate an intense anti-tumor immune response *in vivo* [110].

6. Conclusion and outlook

In this review, we summarized recent advances of TPA-AIEgens for cancer theranostics. Compared to clinical photoactive agents, TPA-AIEgens shows unique and excellent advantageous such as bright emission, robust ROS generation, high photothermal conversion efficacy, resulting in improved antitumor efficacy. By rational design, TPA-AIEgens demonstrate NIR II absorption/emission, enhanced phototherapy. Owing to AIE characteristics, TPA-AIEgens is available to visualize the tumor foci, which plays a vital role in the clinic diagnosis and image-guided surgeons. Moreover, the PDT and PTT combined with immunotherapy, could be a promising approach to enhance the immunotherapy efficiency (Table 1).

Despite impressive advancements of TPA-AIEgens in the realm of biomedicine, there are still certain problems and challenges for clinical application. First, TPA-AIEgens suffer from poor targeting capability of tumors and the accumulation of TPA-AIEgens mainly relies on the EPR effect. By modifying the size, shape, structure, surface charge and target ligands of nanovehicles [113–115], it will be possible to create TPA-AIEgens photoactivators furnishing with unique active targeting properties for accurate and effective antitumor treatment in future. Second, the relationship between structure and target properties of TPA-AIEgens should be systematically studied, which will provide theoretical guidance for further development of the TPA-AIEgens to fulfill clinical requirements. Third, most of the excitation wavelengths of TPA-AIEgens are in the visible range. Compared to those dyes with an absorption in the NIR biological window, TPA-AIEgens encounter the challenges in imaging of deep tissue and high resolution requiremen [116–118]. Besides, TPA-AIEgens, as the photoactive agents, still require rigorous investigation on the therapeutic immunological mechanism and *in vivo* ADMET (absorption, distribution, metabolism, excretion and toxicity) properties. Different strategies including the

structure design of the probes which have been discussed in Section 3, have achieved substantial developments and will definitely promote their transition by addressing the clinical concerns [107,119]. Last but not least, biosafety issues are inevitable for the development of novel TPA-AIEgens. Biodegradability and long-term toxicity to humans must be considered to meet the demands of clinical translation. Consequently, in order to achieve the therapeutic effect of totally curing malignancies and successfully preventing tumor metastasis and recurrence, it is imperative to conduct in-depth research on TPA-AIEgens through the aforementioned aspects. In future research, the biomedical application of TPA-AIEgens in tumor diagnosis and treatment systems can be vigorously promoted.

Declaration of competing interest

The authors declare that they have no known competing financial interests or personal relationships that could have appeared to influence the work reported in this paper.

Acknowledgments

This research was funded by the Hainan Provincial Joint Project of Sanya Yazhou Bay Science and Technology City (No. 820LH027), the Hainan Provincial Natural Science Foundation of China (No. 823RC472), the Open Project Program of Wuhan National Laboratory for Optoelectronics (No. 2021WNLOKF008), the Hainan University Scientific Research Foundation (No. KYQD(ZR)19107), Natural Science Research Talent Project of Hainan Medical University (No. JBGS202101), Hainan Province Clinical Medical Center (2021), Project for Functional Materials and Molecular Imaging Science Innovation Group of Hainan Medical University.

Supplementary materials

Supplementary material associated with this article can be found, in the online version, at doi:10.1016/j.cclet.2023.108934.

References

[1] H. Sung, J. Ferlay, R.L. Siegel, et al., CA Cancer J. Clin. 71 (2021) 209–249.
[2] J. Zhou, G. Yu, F. Huang, Chem. Soc. Rev. 46 (2017) 7021–7053.
[3] Y.C. Zhang, C.X. Liu, C.J. Wu, L.J. Song, Biomed. Pharmacother. 159 (2023) 114257.
[4] D.P. Chen, Q. Xu, W.J. Wang, et al., Small 17 (2021) 2006742.
[5] J.F. Lovell, T.W.B. Liu, J. Chen, G. Zheng, Chem. Rev. 110 (2010) 2839–2857.
[6] Z.Y. Zhuang, J. Dai, M.X. Yu, et al., Chem. Sci. 11 (2020) 3405–3417.
[7] J.Y. Kou, D. Dou, L.M. Yang, Oncotarget 8 (2017) 81591–81603.
[8] K.R. Deng, C.X. Li, S.S. Huang, et al., Small 13 (2017) 1702299.
[9] T.T. Hu, Z.D. Wang, W.C. Shen, et al., Theranostics 11 (2021) 3278–3300.
[10] X.H. Huang, I.H. El-Sayed, W. Qian, M.A. El-Sayed, J. Am. Chem. Soc. 128 (2006) 2115–2120.
[11] F. Chen, W.B. Cai, Nanomedicine 10 (2015) 1–3.
[12] K. Richter, M. Haslbeck, J. Buchner, Mol. Cell 40 (2010) 253–266.
[13] S. Farivar, T. Malekshahabi, R. Shiari, J. Lasers Med. Sci. 5 (2014) 58–62.
[14] K. Xiong, F.M. Wei, Y. Chen, et al., Small 7 (2022) 1702299.
[15] G. Yi, S.H. Hong, J. Son, et al., Quant. Imaging Med. Surg. 8 (2018) 433–443.
[16] Q.F. Xiao, X.P. Zheng, W.B. Bu, et al., J. Am. Chem. Soc. 135 (2013) 13041–13048.
[17] J.J. Wang, X.Z. Peng, J.S. Wei, et al., Nano Today 50 (2023) 101864.
[18] J. Luo, Z. Xie, J.W. Lam, et al., Chem. Commun. 18 (2001) 1740–1741.
[19] Y.C. Chen, J.W.Y. Lam, R.T.K. Kwok, et al., Mater. Horizons 6 (2019) 428–433.
[20] N.L.C. Leung, N. Xie, W.Z. Yuan, et al., Chemistry 20 (2014) 15349–15353.
[21] D. Broadwater, H.C.D. Medeiros, R.R. Lunt, S.Y. Lunt, Annu. Rev. Biomed. Eng. 23 (2021) 29–60.
[22] Y.W. Yu, Y.B. Liu, Y.T. Chen, et al., Mat. Chem. Front. 7 (2022) 96–105.
[23] J. Tavakoli, A.J. Ghahfarokhi, Y.H. Tang, Top. Curr. Chem. (2021) 247–286.
[24] H. Chen, Y.P. Wan, X. Cui, et al., Adv. Healthc. Mater. 10 (2021) 2101607.
[25] Y.Q. Wang, B.Z. Xia, Q.N. Huang, et al., Adv. Healthc. Mater. 10 (2021) 2100945.
[26] J.J. Wang, J.S. Wei, Y.H. Leng, et al., Biosensors 13 (2023) 324.
[27] Z.J. Zhang, W.H. Xu, M.M. Kang, et al., Adv. Mater. 32 (2020) 2003210.
[28] M. Gao, B.Z. Tang, Drug Discov. Today 22 (2017) 1288–1294.
[29] Q. Ma, X. Sun, W. Wang, et al., Chin. Chem. Lett. 33 (2022) 1681–1692.
[30] L. Liu, J. Ma, J.M. Pan, et al., New J. Chem. 45 (2021) 5049–5059.
[31] L.F. Xu, F.Z. Xiong, M.Q. Kang, et al., Analyst 147 (2022) 4132–4140.
[32] S. Suzuki, S. Sasaki, A.S. Sairi, et al., Angew. Chem. Int. Ed 59 (2020) 9856–9867.
[33] G.X. Feng, G.Q. Zhang, D. Ding, Chem. Soc. Rev. 49 (2020) 8179–8234.
[34] R. Qu, X. Zhen, X.Q. Jiang, CCS Chem. 4 (2022) 401–419.
[35] T.Y. Wu, J.B. Huang, Y. Yan, Cell Rep. Phys. Sci. 3 (2022) 100771.
[36] G.X. Feng, B. Liu, Small 12 (2016) 6528–6535.
[37] J.X. Liu, W.T. Chen, C.Y. Zheng, et al., Eur. J. Med. Chem. 244 (2022) 114843.
[38] M.J. Jiang, R.T.K. Kwok, X.S. Li, et al., J. Mat. Chem. B 6 (2018) 2557–2565.
[39] J. Dai, X. Wu, S.Y. Ding, et al., J. Med. Chem. 63 (2020) 1996–2012.
[40] T.C. Bozeman, K.A. Edwards, K.M. Fecteau, et al., J. Inorg. Organomet. Polym. Mater. 21 (2011) 316–326.
[41] S.J. Liu, C. Chen, Y.Y. Li, et al., Adv. Funct. Mater. 30 (2020) 1908125.
[42] A.Y. Ji, H.Y. Lou, C.R. Qu, et al., Nat. Commun. 13 (2022) 3815.
[43] T.X. Liu, L.P. Zhu, C. Zhong, et al., Adv. Funct. Mater. 27 (2017) 1606384.
[44] Y. Li, Z. Cai, S. Liu, et al., Nat. Commun. 11 (2020) 1255.
[45] G. Yang, J.S. Ni, Y. Li, et al., Angew. Chem. Int. Ed. 60 (2021) 5386–5393.
[46] S.H. Liu, X. Zhou, H. Zhang, et al., J. Am. Chem. Soc. 141 (2019) 5359–5368.
[47] D. Wang, M.M.S. Lee, W. Xu, et al., Angew. Chem. Int. Ed. 58 (2019) 5628–5632.
[48] H.S. Choi, S.L. Gibbs, J.H. Lee, et al., Nat. Biotechnol. 31 (2013) 148–153.
[49] M.L. Li, J. Xia, R.S. Tian, et al., J. Am. Chem. Soc. 140 (2018) 14851–14859.
[50] W. Xu, Z.B. Zeng, J.H. Jiang, et al., Angew. Chem. Int. Ed. 55 (2016) 13658–13699.
[51] W.J. Li, Y.P. Zhang, Y.C. Wang, et al., Chin. Chem. Lett. 32 (2021) 1571–1574.
[52] H. Zhao, N. Li, C. Ma, et al., Chin. Chem. Lett. 34 (2023) 107699.
[53] Q. Xiao, X. Zhao, H. Xiong, Chin. Chem. Lett. 32 (2021) 1687–1690.
[54] H. Hyun, M.H. Park, E.A. Owens, et al., Nat. Med. 21 (2015) 192–197.
[55] R.W. Horobin, F. Rashid-Doubell, J. Pediani, D.G.. Milligan, Biotech. Histochem. 88 (2013) 440–460.
[56] Y. Li, J. Zhuang, Y. Lu, et al., ACS Nano 15 (2021) 20453–20465.
[57] Y.F. Zhong, H. Zhang, G. Mu, et al., Inorg. Chem. Front. 6 (2019) 2817–2823.
[58] K.N. Wang, L.Y. Liu, D. Mao, et al., Angew. Chem. Int. Ed. 61 (2022) e202114600.
[59] N. Niu, Y. Yu, Z.J. Zhang, et al., Chem. Sci. 13 (2022) 5929–5937.
[60] G. Ding, J. Tong, J. Gong, et al., J. Mater. Chem. B 10 (2022) 5272–5278.
[61] H.F. Wen, Z.C. Zhang, M.M. Kang, et al., Biomaterials 274 (2021) 120892.
[62] X.H. Chen, N. Niu, D. Li, et al., Adv. Funct. Mater. 33 (2023) 2211571.
[63] H. Zhang, C. He, L. Shen, et al., Chin. Chem. Lett. 34 (2023) 108160.
[64] G. Cheng, J. Zielonka, D. McAllister, et al., Cancer Lett. 365 (2015) 96–106.
[65] Z.Y. Liu, H. Zou, Z. Zhao, et al., ACS Nano 13 (2019) 11283–11293.
[66] Y.B. Wang, S.D. Xu, L.L. Shi, et al., Angew. Chem. Int. Ed. 60 (2021) 14945–14953.
[67] H. Wang, Y.L. Xu, B.S. Xu, et al., Tetrahedron Lett. 61 (2020) 151703.
[68] M. Wang, R.J. Kaufman, Nat. Rev. Cancer 14 (2014) 581–597.
[69] C.G. Towers, A. Thorburn, Cancer Discov. 7 (2017) 1218–1220.
[70] M.Q. Yang, J.R. Deng, H.F. Su, et al., Mat. Chem. Front. 5 (2021) 406–417.
[71] Y.Z. Xu, D.F. Dang, N. Zhang, et al., ACS Nano 16 (2022) 5932–5942.
[72] X.Z. Peng, J.J. Wang, F.F. Zhou, et al., Cell. Mol. Life Sci. 78 (2021) 5139–5161.
[73] J.W. Zhu, J.H. Zou, Z.J. Zhang, et al., Mat. Chem. Front. 3 (2019) 1523–1531.
[74] J. Qi, Y. Fang, R.T.K. Kwok, et al., ACS Nano 11 (2017) 7177–7188.
[75] Y.Q. Huang, K.L. Liu, H.L. Ni, et al., ACS Appl. Polym. Mater. 4 (2022) 7739–7750.
[76] Y. Lu, J. Xu, Z. Jia, et al., Chin. Chem. Lett. 33 (2022) 1589–1594.
[77] Y. Li, J. Cui, C. Li, et al., Chin. Chem. Lett. 34 (2023) 108180.
[78] M.M. Kang, Z.J. Zhang, N. Song, et al., Aggregate 1 (2020) 80–106.
[79] J. Mei, N.L.C. Leung, R.T.K. Kwok, et al., Chem. Rev. 115 (2015) 11718–11940.
[80] X.H. Chen, Y.X. Li, S.W. Li, et al., Adv. Funct. Mater. 28 (2018) 1804362.
[81] C. Wang, X.H. Zhao, H.Y. Jiang, et al., Nanoscale 13 (2021) 1195–1205.
[82] Y. Yang, H. Zhong, B. Wang, et al., Chin. Chem. Lett. 34 (2023) 107674.
[83] Y. Ban, L. Hao, Z. Peng, et al., Chin. Chem. Lett. 34 (2023) 107880.
[84] H. Zou, J. Zhang, C.M. Wu, et al., ACS Nano 15 (2021) 9176–9185.
[85] Y.P. Zhou, W.K. Xia, C. Liu, et al., Biomater. Sci. 10 (2022) 1742–1751.
[86] M. Li, H. Li, Q. Wu, et al., iScience 24 (2021) 102261.
[87] W. Shao, F.L. Zhao, J.H. Xue, L.L. Huang, BMEMat 1 (2023) e12009.
[88] L.H.V. Wang, S. Hu, Science 335 (2012) 1458–1462.
[89] P.P. Liang, Y. Wang, P. Wang, et al., Nanoscale 9 (2017) 18890–18896.
[90] H. Gu, W.J. Liu, W. Sun, et al., Chem. Sci. 13 (2022) 9719–9726.
[91] D. Wang, B.Z. Tang, Accounts Chem. Res. 52 (2019) 2559–2570.
[92] M. Gao, B.Z. Tang, Coord. Chem. Rev. 402 (2020) 213076.
[93] Z.Y. He, S.D. Tian, Y.T. Gao, et al., Front. Chem. 9 (2021) 672917.
[94] J. Ingle, S. Basu, ACS Omega 8 (2023) 8925–8935.
[95] T.J. Dougherty, Semin. Oncol. 11 (1995) 333–334.
[96] Y.C. Ma, Z.Y. Zhuang, L.J. Xing, et al., Adv. Funct. Mater. 31 (2021) 2106988.
[97] X.H. Chen, Z.C. Zhang, W.S. Luo, et al., Biomaterials 287 (2022) 121680.
[98] L.P. Zhao, X. Zhang, X.X. Wang, et al., J. Nanobiotechnol. 19 (2021) 335.
[99] S. Nomura, Y. Morimoto, H. Tsujimoto, et al., Sci. Rep. 10 (2020) 9765.
[100] G.L. He, M.M. He, R. Wang, et al., Angew. Chem. Int. Ed. 62 (2023) e202218768.
[101] D.M. Xi, M. Xiao, J.F. Cao, et al., Adv. Mater. 32 (2020) 1907855.
[102] L. Chen, D. Liu, M.Y. Wu, et al., Nanotechnology 31 (2020) 315101.
[103] M.Q. Yang, S. Cao, X.Z. Sun, et al., Bioconjug. Chem. 31 (2020) 663–672.
[104] J.J. Guo, J. Dai, X.L. Peng, et al., ACS Nano 15 (2021) 20042–20055.
[105] W.T. Sun, X.F. Wang, Z.Y. Cheng, et al., Biomed. Pharmacother. 158 (2023) 114071.
[106] Q. Chen, G.J. Chen, J.W. Chen, et al., Nano Lett. 19 (2019) 4879–4889.

[107] G.X. Lan, K.Y. Ni, Z.W. Xu, et al., J. Am. Chem. Soc. 140 (2018) 5670–5673.
[108] G. Yang, S.B. Lu, C. Li, et al., Chem. Sci. 12 (2021) 14773–14780.
[109] J.Q. Li, J. Dai, Z.Y. Zhuang, et al., Biomaterials 291 (2022) 121899.
[110] Y.Y. Ling, X.Y. Xia, L. Hao, et al., Angew. Chem. Int. Ed. 61 (2022) e202210988.
[111] M. Chen, X.Y. Zhang, J.K. Liu, et al., ACS Nano 14 (2020) 4265–4275.
[112] F. Lv, D.P. Liu, W.H. Zheng, et al., ACS Appl. Nano Mater. 4 (2021) 6012–6019.
[113] T.J. Wang, Z.Y. Gao, Y.F. Zhang, et al., J. Control. Release 351 (2022) 272–283.
[114] F. Hammerer, G. Garcia, S. Chen, et al., J. Org. Chem. 79 (2014) 1406–1417.
[115] Y.C. Chen, W.F. Lee, H.H. Tsai, W.Y. Hsieh, J. Biomed. Mater. Res. Part A 100A (2012) 1279–1292.
[116] Y.Y. Li, J.Q. Zhang, S.J. Liu, et al., Adv. Funct. Mater. 31 (2021) 2102213.
[117] S.B. Lv, Y.H. Liu, Y.L. Zhao, et al., Biomater. Sci. 10 (2022) 4785–4795.
[118] X. Liu, G. Li, M.J. Xie, et al., Dalton Trans. 49 (2020) 11192–11200.
[119] W.L. Liu, M.Z. Zou, T. Liu, et al., Adv. Mater. 31 (2019) 1900499.